TIME MIGRATION VELOCITY ANALYSIS BY IMAGE-WAVE PROPAGATION OF COMMON-IMAGE GATHER

J. Schleicher, J. C. Costa, and A. Novais

email: *js@ime.unicamp.br*

keywords: *Migration velocity analysis, remigration, image-waves, velocity continuation, residual moveout*

ABSTRACT

Image-wave propagation or velocity continuation describes the variation of the migrated position of a seismic event as a function of migration velocity. Image-wave propagation in the common-image gather (CIG) domain can be combined with residual-moveout analysis for iterative migration velocity analysis. Velocity continuation of CIGs leads to a detection of those velocities where events flatten. Although image-wave continuation is based on the assumption of a constant migration velocity, the procedure can be applied in inhomogeneous media. For this purpose, the CIGs obtained by migration with an inhomogeneous macrovelocity model are continued starting from a constant reference velocity. The interpretation of continued CIGs as obtained from residual migrations leads to a correction formula that translates the residual flattening velocities into absolute time-migration velocities. In this way, the migration velocity model can be iteratively improved until a satisfactory result is reached. By means of a numerical example, we show that migration velocity analysis with iterative image continuation exclusively applied to selected common-image gathers is able to construct a reasonable migration velocity model from scratch, without any need of a building an initial model from a previous conventional NMO/DMO velocity analysis.

INTRODUCTION

The quality of a final seismic depth or time migrated image depends on the available velocity information. This fact is independent of the employed migration method. Conventional normal moveout (rms) velocity analysis (Dix, 1955; Yilmaz, 1987) can provide a satisfactory macrovelocity as long as its inherent assumptions of hyperbolic moveout, flat reflectors, and lateral homogeneity are reasonably well satisfied.

In more challenging environments, the conventional velocity model needs to be improved with migration velocity analysis (MVA). In MVA, different migrated images of the same position obtained from different subsets of the data are collected into so-called common-image gathers (CIGs). The CIGs are sensitive to the velocity model (Al-Yahya, 1989). The idea is that for the correct migration velocity, the image of the same subsurface point should be independent of the data subset used to produce it. Thus, the reflection events in a CIG should be flat regardless of the structures (Stork, 1992). On the other hand, for an incorrect migration velocity, different data subsets will lead to different images, thus resulting in nonflat reflection events in the CIG. A more detailed description can be found in Zhu et al. (1998).

Migration velocity analysis has been proposed by many authors. The suggested methods range from a simple comparison of different common-offset images (Gardner et al., 1974) over wavefield extrapolation of CMP gathers (Yilmaz and Chambers, 1984), trial migrations plus stacking (Fowler, 1985), and focusing depth analysis (Faye and Jeannot, 1986), to residual-moveout (RMO) analysis in the offset-domain (Al-Yahya, 1989) or angle-domain (Biondi and Symes, 2004) CIG.

Because of its conceptual clearness and simplicity, RMO analysis has become the favorite tool for MVA. During the years, many improvements have been suggested (Deregowski, 1990; Lee and Zhang,

1992; Lafond and Levander, 1993; Liu and Bleistein, 1995; Liu, 1997; Yan and Lines, 2001; Chauris et al., 2002; Fei and McMechan, 2005, 2006; Schleicher and Biloti, 2007, see also references therein).

A completely different approach to MVA is based on the continuation of a seismic image in velocity. This is a straightforward extension of residual migration (Rothman et al., 1985) or cascaded migration (Larner and Beasley, 1987) to continuous velocity variation (Claerbout, 1986; Fomel, 1994). Goldin (1994) developed a more general theory of image continuation, which he called contact continuation. The kinematics and dynamics of image continuation in the time-migrated domain have been thoroughly discussed by Fomel (2003b). In a companion paper, Fomel (2003a) suggested its use for time-migration velocity analysis in the prestack domain.

In this paper, we combine the concepts of RMO analysis and image continuation, in this way devising a tool for RMO analysis in the form of an FD implementation of a partial differential equation. We provide a simpler derivation for Fomel's (2003b) image-wave equation for direct application in offset-domain CIGs. Letting the reflection events in each CIG propagate until they are flat, we find a velocity value for each identifiable event. After migration with the preliminary model, the procedure can be applied iteratively for residual migration. In this way, we are able to construct an inhomogenous macrovelocity model. We demonstrate this MVA strategy on the Marmousoft data (Billette et al., 2003).

REVIEW OF IMAGE CONTINUATION

When a seismic section is depth- or time-migrated with different (constant) migration velocities, different reflector images of the subsurface are obtained. By continuously changing the migration velocity, the image can be continued in velocity. Based on the kinematics of the dislocation of the image of a seismic event under variation of the migration velocity, Fomel (1994) presented partial differential equations that describe this velocity continuation. Due to the similarity with propagating waves, Hubral et al. (1996b) interpreted the continued images for different velocities as snapshots of propagating "image waves". Consequently, they termed the resulting differential equations "image-wave equations".

In the same way as physical waves propagate as a function of time, these image waves propagate as a function of migration velocity. It is therefore straightforward to associate the moving reflector images with pseudo "wavefronts" that "propagate" as a function of the migration velocity v. This view is taken by Fomel (1994) and Hubral et al. (1996b). Different migrated images can thus be considered as snapshots of image waves at different instants of migration velocity. By some simple plane-wave considerations, image-wave equations can be derived that describe the propagation of image waves as a function of the migration velocity.

Also in correspondence to physical wave propagation, there are pseudo "rays" associated with this image-wave propagation. Such a "velocity ray" (Fomel, 1994) or "image-wave ray" (Schleicher et al., 1997) is given by the set of all possible migrated loci of one point N on a seismic reflection-time surface Γ in the original CMP or ZO section. Which of all possible velocity rays is actually associated with the event is defined by the local slope of Γ at N.

These velocity rays describe the curve through the migrated section that the reflection point of a seismic event with a certain slope describes when the migration velocity is changed continuously. For example, in the case of a CMP stack or zero-offset (ZO) section, the ZO reflection signal moves along a circle at depth, as recognized independently from geometrical considerations by Cognot et al. (1995) and Liptow and Hubral (1995), and mathematically shown by Schleicher et al. (1997). The circle degenerates to a vertical line for a nondipping event. For all other dips, the dislocation as a function of migration velocity depends on the reflector dip. In particular and somewhat counterintuitively, for reflectors with dips larger than 45°, the reflection point moves *upward* for *increasing velocity* (Chun and Jacewitz, 1981).

The corresponding velocity rays in a time-migrated ZO section are parabolas (Liptow and Hubral, 1995; Schleicher et al., 1997). The associated ray-tracing system was presented by Fomel (2003b). More general expressions for velocity rays with nonzero offset in homogeneous media have been derived by Adler et al. (1997) and Adler (2002). Iversen (1996) derived expressions for first-order perturbations of reflection points (i.e., straight velocity rays) situated within a 3D heterogeneous isotropic velocity model. He shows that the partial derivatives of traveltime functions involved in calculating image point displacements in heterogeneous media can be calculated with ray perturbation theory (Farra and Madariaga, 1987). Iversen (2006) found ray-tracing systems for velocity rays involving linear approximations for inhomogeneous

anisotropic media. He provides a theory by which one can obtain velocity rays in 3D models of the subsurface. His approach is numeric, because analytical solutions exist only for very simple velocity models and source-receiver configurations.

A velocity ray has the important property that all image points along the ray belong to the same seismic event. Using this property, Adler (2002) derives a local linear approximation to the velocity ray for perturbations of a 3D laterally inhomogeneous model from the imaging equations. This approximation is valid for arbitrary reflector geometries and arbitrary sourceâĂŞ receiver configurations. The obtained differential image point displacement is tangent to the velocity ray. It is described by a linear equation that contains the Beylkin matrix (Beylkin, 1985) as well as the traveltime and slowness perturbations with respect to the model. This result is equivalent to the description of Iversen (1996). Adler (2002) uses this image point displacement Kirchhoff inversion to predict perturbed images in parallel with the initial image during a single application of migration/inversion with an initial velocity model, in this way indicating a manner of generalizing the concept of image continuation to inhomogeneous media.

The ray approach to image-wave propagation has two advantages over the direct use of the image-wave equations themselves. Firstly, it is much easier to derive the eikonal equation (or Hamiltonian) from the kinematics of a given imaging problem than the corresponding image-wave equation. Secondly, in not too strongly inhomogeneous media, rays are local trajectories that depend only on local values of the involved quantities. Therefore, a generalization to such media is much easier. Note, however, that in the general case, even velocity rays are no longer local quantities but may depend on medium properties far away. As demonstrated by Duchkov et al. (2006), it is nontheless always possible to construct a Hamiltonian for a given propagation problem that is at least microlocally valid, thus permitting an approximate short-distance image propagation.

The dependence of the velocity rays on the original slope of the reflection event has an important consequence. To construct a ray from an initial image, one needs to detect the initial direction for the ray. This, in turn, implies the need for a preliminary image analysis (slant-stack or similar) to detect the local dip. The existence of an image-wave equation (written out in explicit form) allows to avoid this step and solve an initial value problem for the discretized equation, where the image itself is the initial data.

Therefore, when an image-wave equation for a given problem can be found, its direct solution using finite-difference or spectral methods has a more general appeal. It can be used to globally move a migrated image to a new position without the need to identify and pick reflector elements. This might even lead to events coming into focus that cannot previously be identified in the migrated section. Therefore, image-wave equations have been the topic of a number of research papers.

The image-wave equation for ZO (or post-stack) *time* remigration has already been theoretically studied and implemented (Jaya et al., 1996; Jaya, 1997), as well as successfully applied to real data from ground-penetrating radar. In this way, it was possible to find a constant migration velocity (Jaya, 1997; Jaya et al., 1999) or even a laterally varying one (Novais et al., 2008).

The kinematics and dynamics of image continuation in the time-migrated domain have been thoroughly discussed by Fomel (2003b). In a companion paper, Fomel (2003a) suggested its use for time-migration velocity analysis in the prestack domain. He derives image-wave equations for a single CIG and for the full pre-stack data cube. By application to synthetic and field data examples, he concludes that velocity continuation is a powerful method for time-migration velocity analysis, because of its ability to take into account both vertical and lateral movement of the reflection events in seismic images with the changes of migration velocity. Including velocity continuation in the practice of migration velocity analysis can improve the focusing power of time migration and reduce the production time by avoiding the need for iterative velocity refinement. No prior velocity model is required for this type of velocity analysis.

The image-wave equation for ZO *depth* remigration has been studied by Schleicher et al. (2004). They study consistency, stability, and convergence of adequate FD schemes and extend the investigation to grid dispersion and dissipation. After these more technical details, they discuss the potential of the depth remigration image-wave equation as a technique for migration velocity analysis in homogeneous and vertically inhomogeneous media.

There is one problem that all these image-wave equations have in common. It is the principal difficulty to generalize the theory to inhomogeneous media. Although it is conceptually easy to imagine a reflector image to propagate under change of only a part of the overburden velocity model, the mathematical problem behind it is much harder. How could we possibly make the propagation variable of a wave equation

inhomogeneous? A first idea, presented by Audebert et al. (1997), is to avoid this problem by introducing a new propagation variable α that describes the systematic variation of an inhomogeneous model M_1 by $M = \alpha M_1$. Another possible solution was indicated by Duchkov et al. (2007): In the convex combination of two models, $M = \alpha M_1 + (1 - \alpha) M_2$, where $0 < \alpha < 1$, α can become the propagation variable to change continuously from one inhomogeneous model M_1 to another one M_2.

Nonetheless, even constant-velocity image-wave equations have been successfully applied to time and depth migration in inhomogeneous media (Fomel, 2003a,b; Schleicher et al., 2004; Novais et al., 2008). While for constant migration velocity, time and depth migration are completely equivalent problems that can be easily transformed one into the other, the situation is slightly more complicated in inhomogeneous media. Even though the equations are still the same, the meaning of the velocity values as average velocities is different in time and depth. The meaning of a constant average value for the time migration velocity poses no problem since a time-migration velocity is just that, well-known to be a good approximation to the rms velocity in vertically inhomogeneous media, and recently thoroughly investigated in more general media by Cameron et al. (2007). On the other hand, the meaning of a constant average value for the depth migration velocity is somewhat more obscure.

Schleicher et al. (2004) demonstrated that the method, although strictly valid for homogeneous media only, can be applied in vertically inhomogeneous media. Because of the assumption of a constant migration velocity, depth remigration by the image-wave equation could be thought of as a time remigration in pseudo-depth. However, for a horizontally layered model, a reflector image won't reach its true depth if the rms velocity is used for remigration. Instead, a propagating reflector image reaches its true depths at a migration velocity that approximately equals the inverse of the mean slowness. In this way, mean slownesses can be determined from image-wave remigration, thus enabling migration velocity analysis.

Recently, the concept of image continuation has been extended to elliptic anisotropy. Schleicher and Aleixo (2007) and Schleicher et al. (2008) derive time and depth image-wave equations not only in velocity but also in medium ellipticity, demonstrating that it is possible to construct an ellipticity map from well-tie information using partial differential equations to propagate the image from isotropy to anisotropy.

METHODOLOGY

To describe the concept of image continuation mathematically, let us start from the well-known fact that, in seismic migration, a single (possibly identified and picked) reflection-time curve in a common-midpoint (CMP) stack or zero-offset (ZO) section leads to different (depth or time) migrated reflector images when different migration velocities are used. To transform these migrated reflector images from one to another in a direct way, i.e., without going back to the original CMP or ZO section, is a seismic imaging task that can be achieved by a residual or cascaded migration. In this way, an improved seismic reflector image for an improved migration velocity is obtained by applying a migration operator to the already migrated rather then unmigrated section (Jacubowicz and Levin, 1983). Residual migration is based on the fact that the migrated image obtained from migrating a second time (with the migration velocity v_2) a seismic section that has already been migrated (with the migration velocity v_1) is identical to the one that would have been obtained from migrating the original CMP or ZO section once, with the effective migration velocity (Rocca and Salvador, 1982)

$$v_{eff} = \sqrt{v_1^2 + v_2^2}\,. \tag{1}$$

Given the first ("incorrect") migration velocity v_1 and the desired effective ("correct") migration velocity v_{eff}, a residual migration is nothing more than a conventional migration with the residual migration velocity $v_2 = \sqrt{v_{eff}^2 - v_1^2}$ (Rothman et al., 1985). Cascaded migration involves an iterative procedure (Larner and Beasley, 1987). By performing n times a migration with a small velocity increment Δv, the desired effective migration velocity

$$v_{eff} = \sqrt{n \Delta v^2} \tag{2}$$

is finally reached. It is not difficult to accept that by choosing a large number n of steps and a very small velocity increment Δv, a cascaded migration simulates a quasi-continuous change of the migration velocity. This procedure leads to a description by a partial differential equation (Claerbout, 1986). Alternatively, the

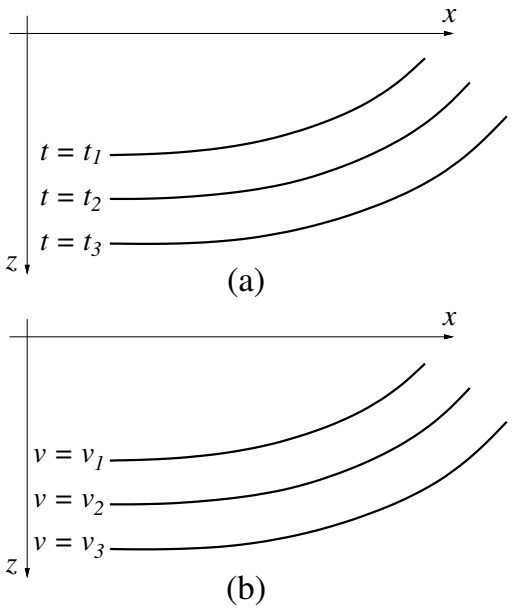

Figure 1: Schematic sketch: (a) Propagating wavefront at three different instants of time. (b) Migrated reflector images for three different migration velocities.

kinematic behavior of different reflector images obtained by migration with different (constant) migration velocities can be used to derive the very same partial differential equation (Fomel, 1994).

When continuously changing the migration velocity, the (kinematically) migrated image of a single point on the reflector, constructed for one particular seismic event, moves to a different position. As a consequence, the reflector image as a whole behaves to some extent like a wavefront of a body wave which can therefore be called image wave (Hubral et al., 1996b).

An image wave is not a physical wave but formally behaves like one. Its concept is best understood with the help of Figure 1. Figure 1a depicts the familiar situation of a propagating (physical) body wave. Three wavefronts of an elementary wave at three different instants of time are indicated. In Figure 1b, another familiar situation is shown that is, however, commonly not viewed as an example of wave propagation. We see three different (purely kinematically) migrated images of one and the same seismic reflector, obtained with three different (constant) migration velocities. By a comparison with the situation depicted in Figure 1a, it is not difficult to accept that this can be conceptually understood as a certain kind of "wave propagation." In the same way as Figure 1a depicts a physical wavefront at three different instants of time, Figure 1b can be said to depict an image wavefront at three different "instants of migration velocity."

In the same way as physical waves propagate as a function of time, these image waves propagate as a function of migration velocity. Different migrated images can thus be considered as snapshots of image waves at different instants of migration velocity. Thus, in the same way as physical wavefronts in Figure 1a can be described by a function $t = T(x, z)$, (where $T(x, z)$ is the eikonal), the depth-migrated reflector image in Figure 1b could be described by a function

$$v = V(x, z) \ , \tag{3}$$

where $V(x, z)$ can be called the image-wave eikonal. Correspondingly, for time migration, the "image-wave front" is described by the image-wave eikonal

$$v = \tilde{V}(x, \tau) \ , \tag{4}$$

where τ is vertical time. Actually, the image-wave eikonals V and $\tilde{V}$ may depend on further parameters like, for instance, the half-offset h or scattering angle θ for which the migration was done, or even anisotropy parameters.

Let the migrated wavefield be represented by $p(x, z, v)$ in depth or by $\tilde{p}(x, \tau, v)$ in time, where the explicit appearance of v in the argument indicates the dependence of the migrated image on the migration

velocity used. As shown by Fomel (1994) and Hubral et al. (1996b), both types of the above image waves for zero offset are then determined by the following partial differential equations

$$\frac{\partial^2 p}{\partial x^2} + \frac{\partial^2 p}{\partial z^2} + \frac{v}{z}\frac{\partial^2 p}{\partial v \partial z} = 0 \ , \tag{5}$$

and

$$\frac{\partial^2 \tilde{p}}{\partial v \partial \tau} + \tau v \frac{\partial^2 \tilde{p}}{\partial x^2} = 0 \ , \tag{6}$$

respectively, which are called "image-wave equations." They can, in turn, be associated with corresponding "image-wave eikonal equations," namely

$$\left(\frac{\partial V}{\partial x}\right)^2 + \left(\frac{\partial V}{\partial z}\right)^2 - \frac{v}{z}\frac{\partial V}{\partial z} = 0 \ , \tag{7}$$

and

$$\frac{\partial \tilde{V}}{\partial \tau} - \tau v \left(\frac{\partial V}{\partial x}\right)^2 = 0 \ , \tag{8}$$

respectively. These differential equations (7) and (8) describe how the propagation of any given image-wave front in a migrated ZO section depends on the changing migration velocity. Using the image-wave equations (5) and (6), any (old) depth-migrated section $p_0 = p(x, z, v_0)$ or time-migrated section $\tilde{p}_0 = \tilde{p}(x, \tau, v_0)$, computed for the migration velocity v_0, can be transformed to the (new) depth-migrated section $p(x, z, v)$, or time-migrated section $\tilde{p}(x, \tau, v)$, computed for the migration velocity v, without having to go back to the original CMP stack or ZO section. In other words, equations (5) and (6), together with initial conditions $p(x, z, v_0) = p_0$ and $\tilde{p}(x, \tau, v_0) = \tilde{p}_0$, respectively, determine the initial-value problems that describe the transformations

$$p(x, z, v_0) \rightarrow p(x, z, v) \ , \tag{9}$$

and

$$\tilde{p}(x, \tau, v_0) \rightarrow \tilde{p}(x, \tau, v), \tag{10}$$

respectively. The initial-value problems for transformations (9) and (10), which represent depth and time remigration, can be solved by spectral, finite-difference, or integral-operator methods (Tygel and Hubral, 1989; Fomel, 1994, 1997, 1998; Hubral et al., 1996a; Tygel et al., 1996; Fomel, 2003a,b; Schleicher et al., 2004; Novais et al., 2008).

The characteristics of the above image-wave eikonal equations are the velocity rays mentioned above (Fomel, 1994; Iversen, 1996). In the ZO case, the characteristics of equations (7) and (8) are circles and parabolas (Liptow and Hubral, 1995; Schleicher et al., 1997). The ray-tracing system associated with equation (8) has been presented by Fomel (2003b). More general expressions for velocity rays with nonzero offset in homogeneous media have been derived by Adler et al. (1997) and Adler (2002).

Fomel (1997, 2003a,b) extended the concept of image continuation to the prestack domain. Again from kinematic considerations, he derived the following expression for the general pre-stack image-wave Hamiltonian equation

$$\frac{\partial \tau}{\partial v} = v\tau \left(\frac{\partial \tau}{\partial x}\right)^2 + \frac{h^2}{v^3 \tau} - \frac{h^2 v}{\tau}\left(\frac{\partial \tau}{\partial x}\right)^2 \left(\frac{\partial \tau}{\partial h}\right)^2 \ . \tag{11}$$

Upon setting $h = 0$, equation (11) reduces to

$$\frac{\partial \tau}{\partial v} = v\tau \left(\frac{\partial \tau}{\partial x}\right)^2 \ , \tag{12}$$

which is the zero-offset Hamiltonian equation that is equivalent to eikonal equation (8). The difference between equations (8) and (12) results from the fact that Fomel (2003b) treats v as an independent variable rather than introducing the image-wave eikonal (4).

On the other hand, upon fixing x, equation (11) reduces to the equation for the residual moveout (RMO) in the CIG (Fomel, 2003b)

$$\frac{\partial \tau}{\partial v} = \frac{h^2}{v^3 \tau} \ . \tag{13}$$

This equation corresponds to an image-wave equation of the form (equation 10 in Fomel, 2003a)

$$\frac{\partial \tilde{p}}{\partial \tau} + \frac{v^3 \tau}{h^2} \frac{\partial \tilde{p}}{\partial v} = 0 \; , \tag{14}$$

which can be used to relocate the reflector image in the CIG as the migration velocity changes, thus enabling a prestack MVA. Fomel (2003a) proposes to combine its solution in the frequency domain with that of the zero-offset equation (12) to dislocate the reflection event in the full data space. In this way, image continuation provides an optimal focusing of the reflection energy by properly taking into account both vertical and lateral movements of reflector images with changing migration velocity.

Recently, the concept of image continuation has been extended to elliptic anisotropy. Schleicher and Aleixo (2007) and Schleicher et al. (2008) derive zero-offset time and depth image-wave equations not only in velocity but also in medium ellipticity. The time image-wave equation generalizes to (Schleicher and Aleixo, 2007)

$$\frac{\partial^2 \tilde{p}}{\partial u \partial \tau} + \tau u \frac{\partial^2 \tilde{p}}{\partial x^2} = 0 \; , \tag{15}$$

where u is the horizontal velocity. In other words, the very same time image-wave equation describes the continuation of a time-migrated image in an elliptically anisotropic medium, with only the propagation variable changing its meaning. This is in agreement with the findings of Alkhalifah and Tsvankin (1995), who observe that time migration in elliptically anisotropic media is independent of the vertical velocity and depends only on the variation of the horizontal velocity.

The depth image-wave equation generalizes to two equations since in depth, the position of the migrated reflector image depends on both the horizontal and the vertical velocities. Parametrizing the medium ellipticity as $\varphi = v^2/u^2$, Schleicher and Aleixo (2007) found the equations

$$\frac{\partial^2 p}{\partial x^2} + \varphi \frac{\partial^2 p}{\partial z^2} + \frac{\varphi v}{z} \frac{\partial^2 p}{\partial v \partial z} = 0 \tag{16}$$

for propagation in vertical velocity v, and

$$\frac{\partial^2 p}{\partial x^2} + \frac{2\varphi^2}{z} \frac{\partial^2 p}{\partial \varphi \partial z} = 0 \tag{17}$$

for continuation in ellipticity φ. Equation (17) allows for propagation of an isotropically migrated image into the anisotropic space. Since it is independent of the vertical velocity v, it can be used even if v is unknown as usually the case after time processing.

On the other hand, equation (17) is not the most convenient solution to the problem. Reparametrizing the medium ellipticity by $\kappa = u/v$, Schleicher et al. (2008) found the even simpler image-wave equation for propagation in vertical velocity v

$$\frac{\partial p}{\partial z} - \frac{\kappa}{z} \frac{\partial p}{\partial \kappa} = 0 \; . \tag{18}$$

This equation even remains valid for ellipticity continuation of a migrated image obtained from nonzero-offset data. Moreover, equation (18) does not depend on the lateral coordinates of the reflection point, nor on the actual values of the horizontal and vertical velocities. Therefore, it can be expected that this equation will work approximately even for inhomogeneous media. Schleicher et al. (2008) demonstrated this for a simple synthetic example. In this way, it is possible to construct an ellipticity map from well-tie information using partial differential equations to propagate the image from isotropy to anisotropy. Of course, generalizations of equations (15) to (17) to prestack data along the lines of Fomel (2003a,b) also can be envisaged.

IMAGE GATHER CONTINUATION

There is a rather simple way of deriving Fomel's (2003a) image-wave equation for offset-domain CIGs. We start from equation 1 of Al-Yahya (1989) that describes the migrated position of a horizontal reflector below a constant-velocity overburden with medium velocity v_m as a function of vertical time τ, half-offset h, and migration velocity v. It reads in our notation

$$\tau = \sqrt{\tau_0^2 + h^2 (1/v_m^2 - 1/v^2)} \; , \tag{19}$$

where τ_0 is vertical time at zero offset, i.e., the true migrated position of the reflector image. When solved for v, equation (19) takes the role of the time-migration image-wave eikonal of equation (4). In this case, this solution is easily done to yield

$$v = \tilde{V}(\tau, h) = 1 \Bigg/ \sqrt{\frac{1}{v_m^2} - \frac{\tau^2 - \tau_0^2}{h^2}} \; . \tag{20}$$

Because of the simplicity of this equation, simple differentiation with respect to τ yields the associate image-wave eikonal equation. It reads

$$\frac{\partial \tilde{V}}{\partial \tau} = -\frac{1}{2}\tilde{V}^3 \left(-\frac{2\tau}{h^2}\right) = \frac{v^3 \tau}{h^2} \; , \tag{21}$$

where we have replaced $\tilde{V}$ by v according to equation (20). Since equation (21) does not depend on the medium velocity v_m nor the zero-offset time τ_0 that pertains to a specific reflector, it represents already the searched-for image-wave eikonal equation. Note that correspondingly, simple derivation of equation (19) with respect to v yields Fomel's (2003b) form of the Hamiltonian equation (equation (13) above).

Since equation (21) is an image-wave eikonal equation or Hamiltonian equation, it could already be used to trace velocity rays in a CIG. However, our purpose is finding an image-wave equation, i.e., a partial differential equation the kinematic behavior of which is described by equation (21). It is easy to see that the simplest equation satisfying this condition is

$$\frac{\partial \tilde{p}}{\partial \tau} + \frac{v^3 \tau}{h^2} \frac{\partial \tilde{p}}{\partial v} = 0 \; . \tag{22}$$

This can be confirmed by substituting a ray-like ansatz for the migrated wavefield $\tilde{p}(\tau, h, v) = p_0(\tau, h) f(v - \tilde{V}(\tau, h))$ in equation (22). The highest-order term in derivatives of the wavelet $f(v)$ provides equation (21). Equation (22) is nothing else but Fomel's (2003a) kinematic RMO equation (image-wave equation (14) above).

The procedure of this section has the advantage of being easily transferred to depth. The depth equivalent of equation (19) reads (Schleicher and Biloti, 2007)

$$z = \sqrt{\frac{v^2}{v_m^2} z_0^2 + \left(\frac{v^2}{v_m^2} - 1\right) h^2} \; , \tag{23}$$

where z_0 is the true depth of the supposedly horizontal reflector, and where z is the migrated pseudo-depth. Equation (23) leads to the eikonal

$$v = V(z, h) = v_m \sqrt{\frac{h^2 + z^2}{h^2 + z_0^2}} \; . \tag{24}$$

To get rid of the medium velocity v_m and the true depth z_0 in favor of a derivative of $V(x, z)$, we write equation (24) as

$$\frac{V(z, h)^2}{h^2 + z^2} = \frac{v_m^2}{h^2 + z_0^2} \; . \tag{25}$$

Taking the derivative of equation (25) with respect to z and isolating the derivative of V yields the image-eikonal equation

$$\frac{\partial V}{\partial z} = \frac{vz}{h^2 + z^2} \; . \tag{26}$$

In analogy to the above, substitution of a ray-like ansatz for the migrated wavefield $p(z, h, v) = p_0(z, h) f(v - V(z, h))$ demonstrates that

$$\frac{\partial p}{\partial z} + \frac{vz}{h^2 + z^2} \frac{\partial p}{\partial v} = 0 \tag{27}$$

is the simplest image-wave equation associated with image eikonal equation (26).

Note that there is no h derivative present in equations (22) or (27). This means that no dislocation of the image in the CIG along the h axis occurs, neither in time nor in depth. This happens because of our initial assumption of a horizontal reflector. It is also consistent with the fact that the residual DMO term of Fomel (2003b) is not present in equation (21). Of course, for an arbitrarily shaped reflector, this is incorrect for dipping parts of the reflector, where the image of a certain reflection point does move in the h direction.

However, as we will see in the numerical examples, the description by equation (22) turns out to be a reasonable approximation for small velocity errors. This is in agreement with the findings of Al-Yahya (1989), who observed that the influence of the dip on the migrated reflector image position decreases with decreasing velocity error. Moreover, to account for larger errors, we propose to smooth the velocity model after its updating so as to enable that the dislocation in the h-direction can be taken care of by the following migration. In this way, iterative application of the image-gather continuation with velocity updates according to equation (1) still yields a high-quality final time-migration velocity model. As mentioned in connection with equation (14), Fomel (2003a) proposes to correct the dislocation in the h-direction using equation (11) on the complete data set rather than equation (22) on single CIGs.

The approximation in equation (23) depends more strongly on the assumption of a constant velocity than its time-domain counterpart (19). Thus, it remains unclear whether the time-domain procedure can be successfully transferred to depth in arbitrarily inhomogeneous media.

ITERATIVE MODEL BUILDING

To use the continuation of a single CIG for the detection of a vertically and laterally varying migration velocity model in spite of its restrictive assumptions of a constant-velocity background and horizontal reflectors, we propose the following iterative procedure:

1. As a first step, migrate the data using some constant velocity v_0 (e.g., water velocity $v_0 = 1500$ m/s for marine data or near-surface velocity for land data) and sort the resulting migrated data into offset-domain CIGs.

2. Then, apply the image continuation starting at v_0 by solving equation (22) as discussed above to selected CIGs.

3. From the obtained cube of time-migrated images, detect the velocities $v_f(\tau)$ at which each of the visible events in each CIG is flattened.

4. From these flattening velocities $v_f(\tau)$, construct a new, inhomogeneous migration velocity model v_{j+1}.

5. Migrate the original data another time, now using this new model.

6. If the CIGs are not yet satisfactorily flat, apply the image continuation once more, again starting at a constant velocity v_c. This may or may not be the same as the original migration velocity v_0, for it only serves as a reference velocity.

7. Loop over steps 3. to 6. until the CIGs are satisfactorily flat.

The first execution of step 4 requires only an interpolation of the obtained flattening velocities so as to cover the whole model. However, its subsequent executions require an additional correction. The reason is that in subsequent iterations, the new flattening velocities $v_f(\tau)$ are obtained from an image continuation which based on the assumption that the preceding time migration was done with a constant migration velocity v_c. Of course, this assumption is wrong from the second iteration on. Thus, the values of the flattening velocities $v_f(\tau)$ have no longer an absolute meaning. Therefore, they cannot be used directly to build a new velocity model.

However, these values still carry some relative information. The differences between $v_f(\tau)$ and v_c are a measure of the differences between the desired migration velocity v_m and the previous migration velocity v_j. Using equation (1), we conclude that a residual migration with a residual velocity v_{res} satisfying

$$v_{\text{res}}^2 = v_m^2 - v_j^2 \tag{28}$$

would have flattened the CIGs. On the other hand, had the nonflat CIGs from the previous migration actually been obtained by a migration with the constant velocity v_c, then the image continuation had been correct and the velocities v_f were the correct migration velocities. In this case, the residual migration to flatten the CIGs would need to be done with a residual velocity $v_{\rm res}$ satisfying

$$v_{\rm res}^2 = v_f^2 - v_c^2 \ . \tag{29}$$

Under the assumption that the two residual velocities of equations (28) and (29) are approximately equal, we find the following expression for the corrected migration velocity:

$$v_m \approx v_{j+1} = \sqrt{v_j^2 + v_f^2 - v_c^2} \ . \tag{30}$$

Equation 30 represents the prescription for the model updating procedure of step 4 in all further iterations.

FINITE-DIFFERENCE SCHEME

Equations (22) and (27) are simple one-dimensional one-way wave equations or advection equations with variable propagation velocity ($c = h^2/v^3\tau$ for equation (22) and $c = (h^2 + z^2)/vz$ for equation (27)). Therefore, both are easily implemented using one of the many unconditionally stable finite-difference (FD) schemes that are available in the literature.

One of these is the implicit second-order FD scheme

$$P_k^{n+1} - \alpha_k \left(P_{k+1}^{n+1} - P_{k-1}^{n+1}\right) = P_k^n + \alpha_k \left(P_{k+1}^n - P_{k-1}^n\right) \ , \tag{31}$$

where $P_k^n = \tilde{p}(\tau_k, v_n)$ or $P_k^n = p(z_k, v_n)$ and

$$\alpha_k = \frac{\beta_k}{4}\left(\frac{\Delta v}{\Delta}\right) \ , \tag{32}$$

with $\Delta = \Delta\tau$ (time) or $\Delta = \Delta z$ (depth) and

$$\beta_k = \frac{h^2}{\bar{v}^3\tau_k} \quad \text{(time)} \qquad \text{or} \qquad \beta_k = \frac{h^2 + z_k^2}{\bar{v}z_k} \quad \text{(depth)}. \tag{33}$$

Scheme (31) is staggered, i.e., evaluated at the cell centers between the grid nodes, in v. Therefore, the value $\bar{v}$ of the present migration velocity must be calculated as its mean at $n+1/2$, i.e., $\bar{v} = (v_{n+1} + v_n)/2$. A von Neumann stability analysis (see, e.g., Strikwerda, 1989) by substitution of $P_k^n = \xi^n \exp(i\Omega\Delta)$ in equation (31) yields the amplification factor

$$\xi = \frac{1 + 2i\alpha_k \sin\Omega\Delta}{1 - 2i\alpha_k \sin\Omega\Delta} \ , \tag{34}$$

from which follows immediately $|\xi| = 1$, i.e., scheme (31) is unconditionally stable. Moreover, the tangent of the half phase of ξ is given by the phase of its numerator, i.e.,

$$\tan(c_s\Omega\Delta v/2) = 2\alpha_k \sin\Omega\Delta \ , \tag{35}$$

where $c_s = c_s(\Delta, \Delta v)$ is the numeric phase velocity realized by the FD scheme. Equation (35) leads to the following third-order approximation of the scheme's phase velocity

$$c_s(\Delta, \Delta v) \approx \beta_k \left[1 - \frac{1}{6}\Omega^2\Delta^2 - \frac{1}{12}\beta_k^2\Omega^2\Delta v^2\right] \ . \tag{36}$$

This means that the intrinsic phase velocity of the propagation is approximated by scheme (31) by the numerical phase velocity β_k, which is then reduced by grid dispersion. The latter is small if $\Delta \ll \sqrt{6}/\Omega$ and $\Delta v \ll 2\sqrt{3}/\beta_k\Omega$. Thus, to avoid grid dispersion, reasonable choices for the increments are $\Delta = 1/\Omega_{\rm max}$ and $\Delta v = \Delta/\beta_{\rm max}$, where $\Omega_{\rm max}$ is the largest frequency associated with the vertical axis in the data, and where $\beta_{\rm max}$ is the largest value of β_k that will be considered in the FD calculations.

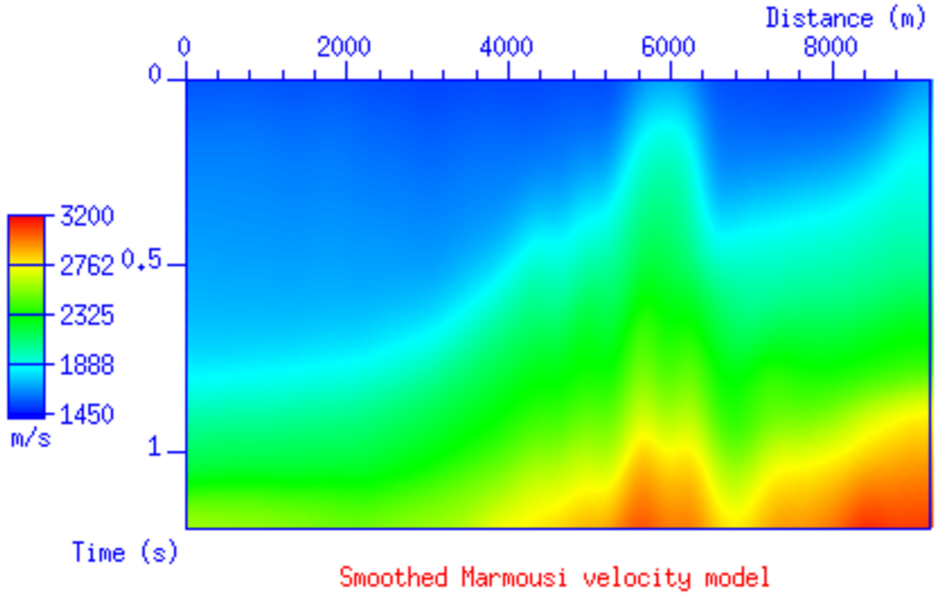

Figure 2: Time velocity model computed from the exact Marmousi model by vertical depth-to-time conversion.

NUMERICAL EXAMPLES

To demonstrate the iterative velocity updating technique suggested above, we applied it to the Marmousoft data (Billette et al., 2003). These synthetic data are obtained by Born modeling in a smoothed version of the original Marmousi model. The smoothing is done using a Gaussian filter with correlation-length $\tau = 240\ m$ (Billette et al., 2003). For comparison with the results of the present technique, we stretched the original Marmousi velocity model to time using the SU routine velconv (Cohen and Stockwell, 2006). The resulting time-velocity model is depicted in Figure 2.

We started by time-migrating the Marmousoft data with the water velocity of $v_0 = 1500$ m/s and sorting the resulting migrated data into offset-domain CIGs. We used a Kirchhoff time migration with an output grid of $\Delta x = 12$ m e $\Delta\tau = 0.002$ s. We then applied the image continuation as discussed above to 95 selected CIGs to propagate them in velocity down to 1400 m/s and up to 3500 m/s. For the FD computations, we used $\Delta v = 25$ m/s and saved every second snapshot. Figure 3 shows 5 of the resulting snapshots of the CIG at 5200 m for velocities 1500 m/s to 3500 m/s at every 500 m/s. It is instructive to see how different events become horizontal at different velocities.

To decide at which velocity v_f each of the visible events in each CIG was flattened, we used velocity semblance spectra along horizontal lines. Figure 4 depicts such a velocity spectrum for the CIG at 5200 m. From the maxima of these velocity spectra, we determined 95 velocity-time functions $v_1(\tau)$. Since this was only the first iteration, we took no care for utmost precision when picking the semblance maxima. From the so-obtained 95 velocity-time functions, we constructed a new, inhomogeneous migration velocity model by B-splines interpolation. This first velocity model is shown in Figure 5. A comparison to Figure 2 reveals a rather good recovery on the right side of the model, but a poorer one on the left side.

Then, we time-migrated the data again using the new velocity model. Figure 6 depicts the resulting migrated image. The faults are already clearly visible and the overall structure of the model can be inferred. Some interfering events indicate that the model can still be improved, particularly in the central part of the image.

As expected because of the restrictive assumptions of a constant-velocity background and horizontal reflectors, the flattening velocities are no perfect migration velocities. Thus, while the second time migration using the so-constructed model is much better than the original time-migrated image using a constant migration velocity, it still leaves room for improvement.

To remedy the situation, we repeated the image continuation after the second time-migration with the

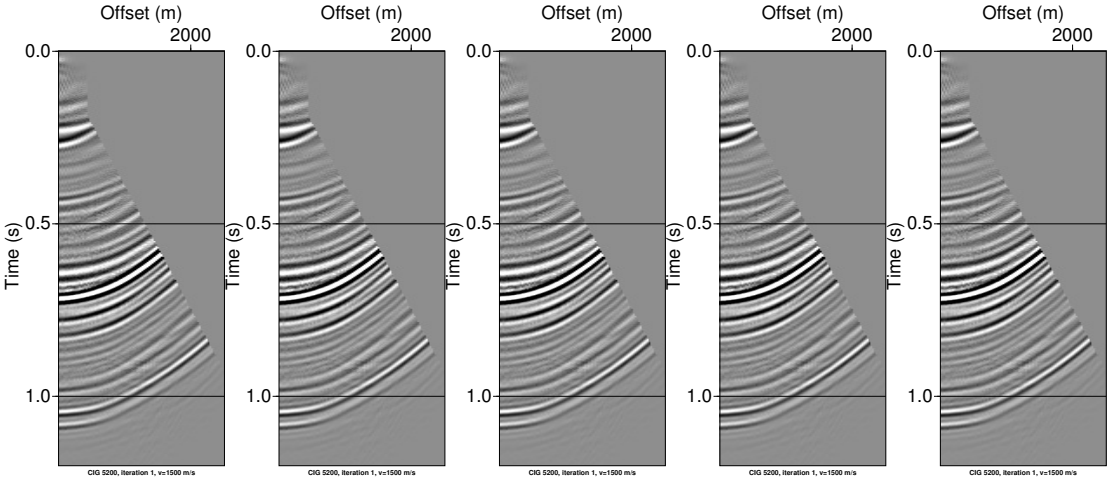

Figure 3: CIG 5200 at velocities 1500 m/s (migration velocity), 2000 m/s, 2500 m/s, 3000 m/s, and 3500 m/s.

new velocity model. In order to use the migration velocity as the propagation variable in the image continuation, we treated the CIGs again as if obtained with a constant reference velocity v_c. To be able to correct for over- and undermigration, we applied two residual image continuations. For the reference velocity, we chose the value of $v_c = 2000$ m/s in order to avoid too large velocity differences to the background model. This choice is rather arbitrary since the principle does not depend on the actual value of v_c. From this reference velocity, we continued the CIGs to larger velocities up to 2500 m/s and to lower velocities down to 1500 m/s in steps of $\Delta v = 10$ m/s. Corresponding snapshots for the CIG at 5200 m are depicted in Figure 7. Note that the central image gather at 2000 m/s is the uncontinued one as obtained directly from migration with the inhomogeneous velocity model of Figure 5. The flattening of events occurs mainly in the velocity range between 1800 m/s and 2200 m/s, indicating that the velocity model is not too bad but can be further improved.

Again, we constructed velocity spectra to decide more precisely at which velocity v_f an event was flattened (see Figure 8). Now, the values of the flattening velocity v_f are residual velocities that are subject to a correction according to equation (30). After correction, we obtained again 95 velocity-time functions $v_2(\tau)$, from which we then constructed an inhomogeneous model with B-splines.

We repeated this procedure until we were satisfied with the result. After a total of five iterations, the velocity model has improved quite reasonably (see Figure 9). The most important features of the time-migration velocity model have been correctly recovered.

The resulting time-migrated image (see Figure 10) also shows the improvement. The reflector continuity in the shallow part has improved. The major difference is in the center part of the image, where the conflicting events have been almost completely resolved. Note that due to the rather complex structure, time migration cannot be expected to produce a much better image of the central part than the one in Figure 10. The CIGs are nicely flattened almost everywhere in the model, particularly in the upper part of the model (see Figure 11). Only a very small number of events show some remaining residual moveout. This is due to the small number of nodes used for the B-splines representation, which thus does not allow for small-scale variations in the resulting velocity model. The CIG at 6400 m demonstrates the difficulties of the process in the complex center part, where crossing events difficult the detection of reliable velocities.

CONCLUSIONS

Residual moveout (RMO) analysis is a tool that has been successfully applied for migration velocity analysis (MVA) by many authors. Image-wave propagation or velocity continuation is a much younger topic that describes the variation of the migrated position of a seismic event as a function of migration velocity.

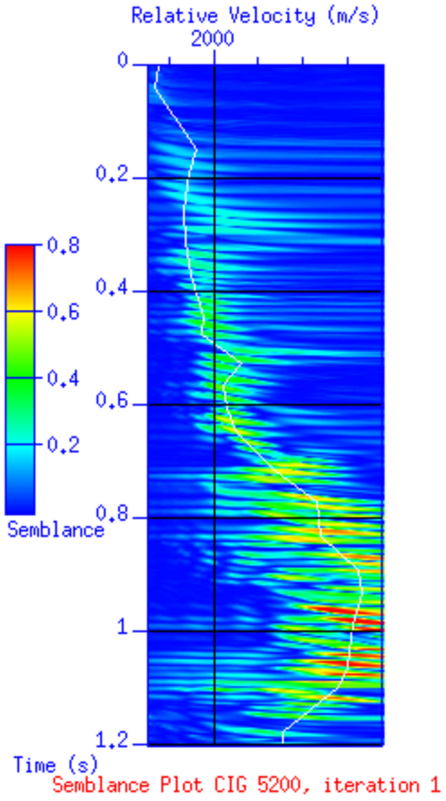

Figure 4: Velocity spectrum obtained from the set of continued CIGs. Also shown is the velocity profile interpreted at this location.

In this paper, we have demonstrated how to construct a tool for RMO analysis based on the approximate image-wave propagation in the common-image gather (CIG) domain. In this way, we have devised an iterative MVA procedure.

We started from a simplified derivation of the image-wave equation in a single CIG based on the kinematic behavior of the image of a single horizontal reflector in a homogeneous medium. This image-wave equation describes the position of the reflector image as a function of migration velocity. Thus, it can be used for a velocity continuation of CIGs to detect those velocities where events flatten.

Although the underlying differential equation describing the image-wave continuation is based on the assumption of a constant migration velocity and a horizontal reflector, the procedure can be applied in more general situations. For this purpose, the CIGs obtained by migration with an inhomogeneous macrovelocity model are continued from a constant reference velocity. Since the error of the approximation decreases with the velocity error, this reference velocity should be chosen somewhere in the middle of the expected velocity range. The continued CIGs can then be interpreted as if obtained from residual migrations. This interpretation leads to a correction formula that translates the residual flattening velocities into absolute time-migration velocities. In this way, the migration velocity model can be iteratively improved until a satisfactory result is reached. In order to reduce the risk of nonconvergence of the so-called Deregowski loop, i.e., local velocity corrections without global improvement, the velocity model should be smoothed between iterations.

By means of a numerical example using the Marmousoft data set, we have demonstrated that migration velocity analysis with iterative image continuation exclusively applied to selected common-image gathers is able to construct a reasonable migration velocity model from scratch, without any need of building an initial model from a previous conventional NMO/DMO velocity analysis.

ACKNOWLEDGMENTS

We thank Gilles Lambaré and Pascal Podvin for making the Marmousoft data set available to us. This work was kindly supported by CNPq and FAPESP, Brazil, and the sponsors of the *Wave Inversion Technology*

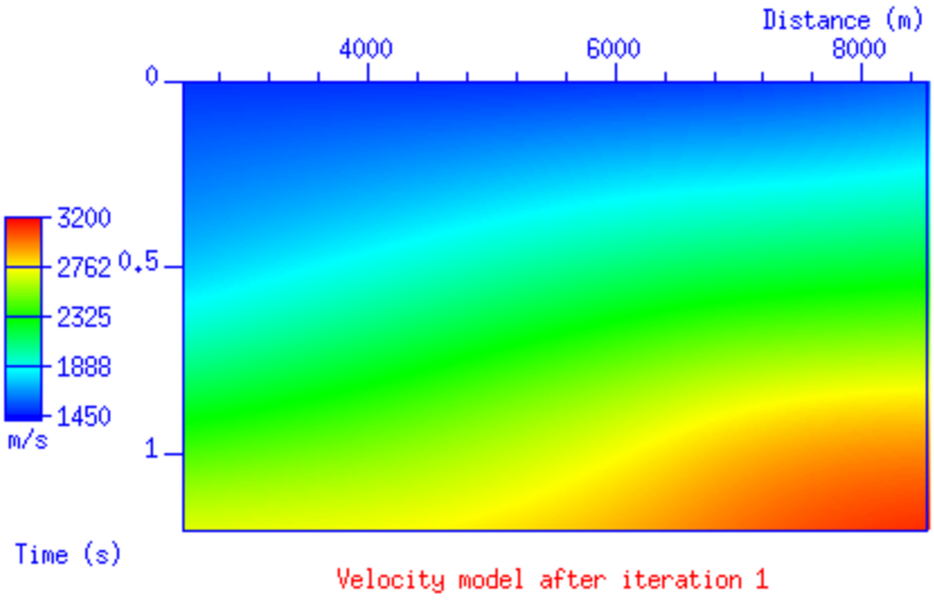

Figure 5: Velocity model extracted using image-wave RMO correction from constant-velocity migration.

(WIT) Consortium.

REFERENCES

Adler, F. (2002). Kirchhoff image propagation. *Geophysics*, 67(1):126–134.

Adler, F., Hoxha, F., and Hubral, P. (1997). Migrating around in circles, part II. *The Leading Edge*, 16:235–237.

Al-Yahya, K. M. (1989). Velocity analysis by iterative profile migration. *Geophysics*, 54(06):718–729.

Alkhalifah, T. and Tsvankin, I. (1995). Velocity analysis for transversely isotropic media. *Geophysics*, 60(05):1550–1566.

Audebert, F., Diet, J., Guillaume, P., Jones, I. F., and Zhang, X. (1997). CRP-scans: 3-D preSDM velocity analysis via zero-offset tomographic inversion. In *67th Ann. Internat. Mtg., SEG, Expanded Abstracts*, pages 1805–1808. SEG.

Beylkin, G. (1985). Imaging of discontinuities in the inverse scattering problem by inversion of a generalized Radon transform. *Journal of Mathematical Physics*, 26(1):99–108.

Billette, F., Le Begat, S., Podvin, P., and Lambare, G. (2003). Practical aspects and applications of 2D sterotomography. *Geophysics*, 68(3):1008–1021.

Biondi, B. and Symes, W. W. (2004). Angle-domain common-image gathers for migration velocity analysis by wavefield-continuation imaging. *Geophysics*, 69(5):1283–1298.

Cameron, M. K., Fomel, S. B., and Sethian, J. A. (2007). Seismic velocity estimation from time migration. *Inverse Problems*, 23:1329–1369.

Chauris, H., Noble, M. S., Lambaré, G., and Podvin, P. (2002). Migration velocity analysis from locally coherent events in 2-D laterally heterogeneous media, Part I: Theoretical aspects. *Geophysics*, 67(4):1202–1212.

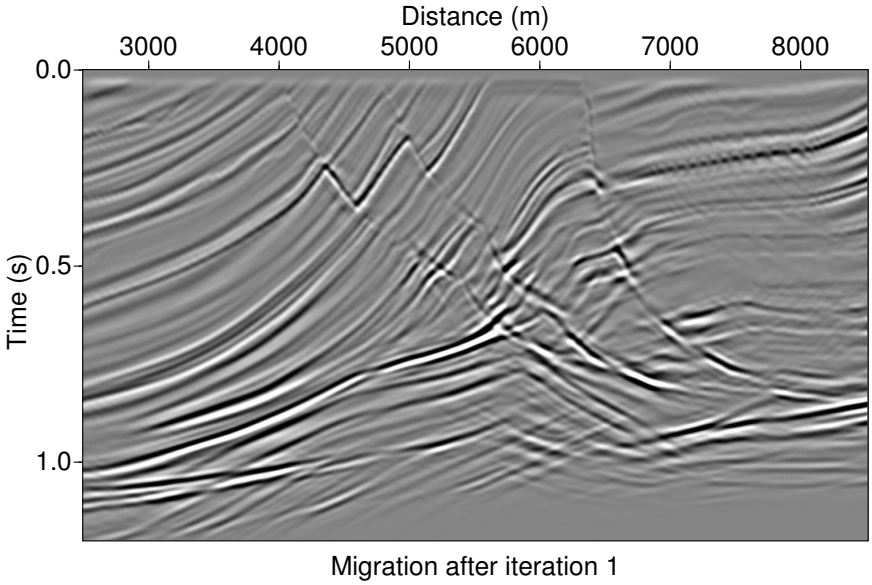

Figure 6: Migrated image after velocity extraction using image-wave RMO correction from constant-velocity migration.

Chun, J. H. and Jacewitz, C. A. (1981). Fundamentals of frequency domain migration. *Geophysics*, 46(5):717–733.

Claerbout, J. (1986). Velocity extrapolation by cascaded 15 degree migration. *Stanford Exploration Project*, SEP-48:79–84.

Cognot, R., Thore, P., and Haas, A. (1995). Tying seismic to well data using structural uncertainties. In Harlan, W. S., editor, *Proceedings*, Tulsa, OK. SEG.

Cohen, J. K. and Stockwell, J. J. W. (2006). Cwp/su: Seismic un*x release no. 40: An open source software package for seismic research and processing. Center for Wave Phenomena, Colorado School of Mines.

Deregowski, S. M. (1990). Common-offset migrations and velocity analysis. *First Break*, 08(06):224–234.

Dix, C. H. (1955). Seismic velocities from surface measurements. *Geophysics*, 20:68–86.

Duchkov, A. A., de Hoop, M. V., Barreto, A. S., and Anderson, F. (2007). Velocity continuation of common-image point gathers using wave packets. In *77th Ann. Internat. Mtg., SEG*, pages 2368–2372. SEG.

Duchkov, A. A., de Hoop, M. V., and Fomel, S. (2006). Continuation of a class of seismic processors and associated âĂŸraysâĂŹ. In *76th Ann. Internat. Mtg., SEG*, pages 2549–2553. SEG.

Farra, V. and Madariaga, R. (1987). Seismic waveform modeling in heterogeneous media by ray perturbation theory. *J. Geophys. Res.*, 92:2697–2712.

Faye, J.-P. and Jeannot, J.-P. (1986). Prestack migration velocities from focusing depth analysis. In *56th Ann. Internat. Mtg., SEG*, pages 438–440. SEG.

Fei, W. and McMechan, G. A. (2005). Fast model-based migration velocity analysis and reflector shape estimation. *Geophysics*, 70(2):U9–U17.

Fei, W. and McMechan, G. A. (2006). 3D common-reflection-point-based seismic migration velocity analysis. *Geophysics*, 71(5):S161–S167.

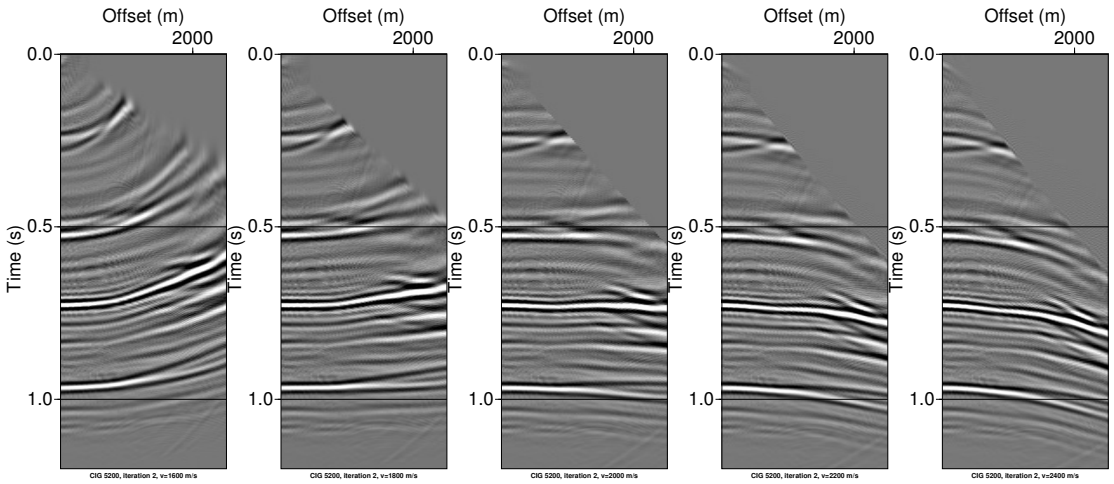

Figure 7: CIG 5200 at velocities 1600 m/s, 1800 m/s, 2000 m/s (which corresponds to the inhomogeneous migration velocity), 2200 m/s, and 2400 m/s after first velocity estimate using image-wave CIG continuation.

Fomel, S. (1994). Method of velocity continuation in the problem of seismic time migration. *Russian Geology and Geophysics*, 35(5):100–111.

Fomel, S. (1997). Migration and velocity analysis by velocity continuation. *Stanford Exploration Project*, SEP-92:161–191.

Fomel, S. (1998). Velocity continuation by spectral methods. *Stanford Exploration Project*, SEP-97:157–172.

Fomel, S. (2003a). Time migration velocity analysis by velocity continuation. *Geophysics*, 68(5):1662–1672.

Fomel, S. (2003b). Velocity continuation and the anatomy of residual prestack time migration. *Geophysics*, 68(5):1650–1661.

Fowler, P. (1985). Migration velocity analysis by optimization: Linear theory. *SEP Report*, 44:1–20.

Gardner, G. H. F., French, W. S., and Matzuk, T. (1974). Elements of migration and velocity analysis. *Geophysics*, 39(06):811–825.

Goldin, S. V. (1994). Superposition and continuation of transformations used in seismic migration. *Russian Geology and Geophysics*, 35(9):109–121.

Hubral, P., Schleicher, J., and Tygel, M. (1996a). A unified approach to 3-D seismic reflection imaging – Part I: Basic concepts. *Geophysics*, 61(3):742–758.

Hubral, P., Tygel, M., and Schleicher, J. (1996b). Seismic image waves. *Geophysical Journal International*, 125(2):431–442.

Iversen, E. (1996). Derivatives of reflection point coordinates with respect to velocity parameters. *Pure and Applied Geophysics*, 148(1/2):287–317. Presented at the Workshop on Seismic Waves in Laterally Inhomogeneous Media, Třešt'.

Iversen, E. (2006). Velocity rays for heterogeneous anisotropic media: Theory and implementation. *Geophysics*, 71(5):T117–T127.

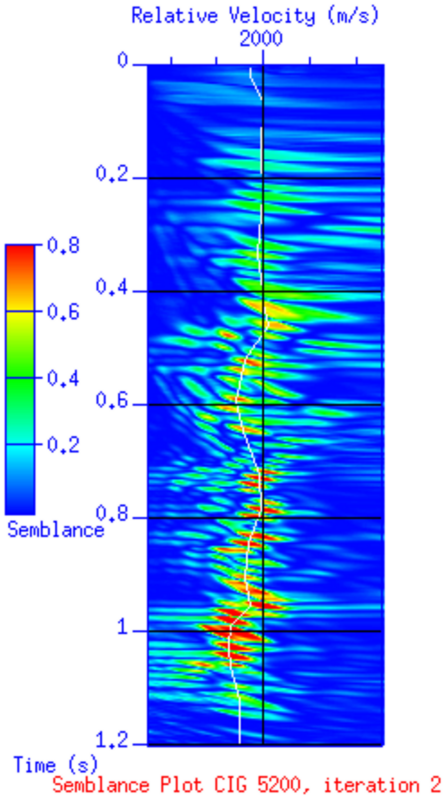

Figure 8: Velocity spectrum obtained from the set of continued CIGs. Also shown is the velocity profile interpreted at this location. These velocity values are corrected with equation (30) to provide the new velocity-time function.

Jacubowicz, H. and Levin, S. (1983). A simple exact method of 3-D migration. *Geophysical Prospecting*, 31:34–56.

Jaya, M. S. (1997). *Imaging reflection seismic data using the method of velocity continuation*. PhD thesis, Universität Karlsruhe (TH).

Jaya, M. S., Botelho, M., Hubral, P., and Liebhardt, G. (1999). Remigration of ground-penetrating radar data. *Journal of Applied Geophysics*, 41:19–30.

Jaya, M. S., Schleicher, J., and Hubral, P. (1996). Post-stack time-domain remigration. In *58th Ann. Internat. Mtg., EAGE*, page X017, Amsterdam. EAEG.

Lafond, C. F. and Levander, A. R. (1993). Migration moveout analysis and depth focusing. *Geophysics*, 58(01):91–100.

Larner, K. and Beasley, C. (1987). Cascaded migration: Improving the accuracy of finite-difference migration. *Geophysics*, 52(5):618–643.

Lee, W. B. and Zhang, L. (1992). Residual shot profile migration. *Geophysics*, 57(06):815–822.

Liptow, F. and Hubral, P. (1995). Migrating around in circles. *The Leading Edge*, 14(11):1125–1127.

Liu, Z. (1997). An analytical approach to migration velocity analysis. *Geophysics*, 62(04):1238–1249.

Liu, Z. and Bleistein, N. (1995). Migration velocity analysis: Theory and an iterative algorithm. *Geophysics*, 60(01):142–153.

Novais, A., Costa, J., and Schleicher, J. (2008). GPR velocity determination by image-wave remigration. *Journal of Applied Geophysics*, 65(2):65–72.

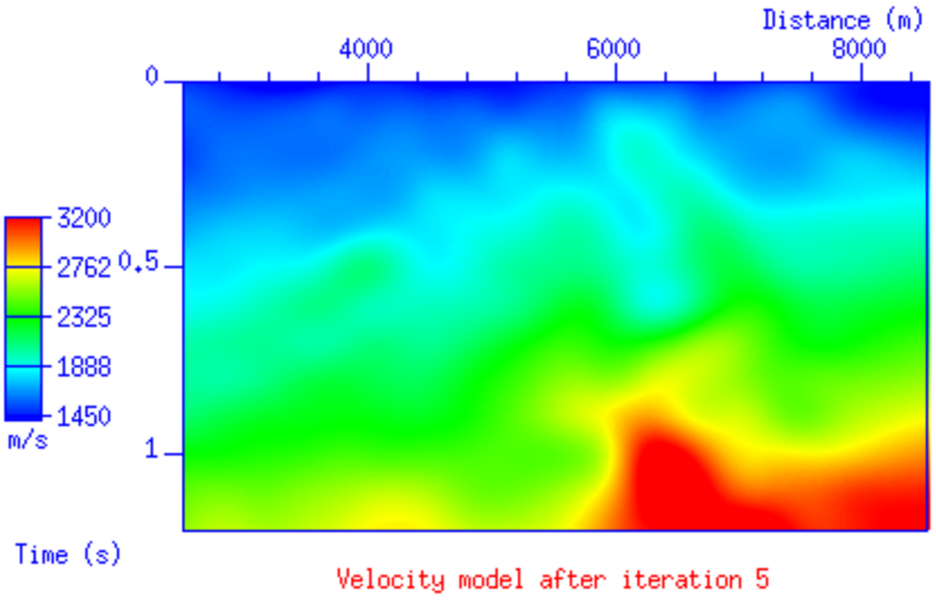

Figure 9: Final velocity model extracted using five iterations of image-wave RMO correction.

Rocca, F. and Salvador, L. (1982). Residual migration. In *52nd Ann. Internat. Mtg., SEG, Expanded Abstracts*, pages S1.4:4–7, Dallas. SEG.

Rothman, D., Levin, S., and Rocca, F. (1985). Residual migration: Applications and limitations. *Geophysics*, 50(1):110–126.

Schleicher, J. and Aleixo, R. (2007). Time and depth remigration in elliptically anisotropic media using image-wave propagation. *Geophysics*, 72:S1–S9.

Schleicher, J., Hubral, P., Höcht, G., and Liptow, F. (1997). Seismic constant-velocity remigration. *Geophysics*, 62(1):589–597.

Schleicher, J., Novais, A., and Costa, J. (2008). Vertical image waves in elliptically inhomogeneous media. *Studia Geophysica et Geodaetica*, 52(1):101–122.

Schleicher, J., Novais, A., and Munerato, F. P. (2004). Migration velocity analysis by depth image-wave remigration: First results. *Geophysical Prospecting*, 52:559–573.

Schleicher, J. and Biloti, R. (2007). Dip correction for coherence-based time migration velocity analysis. *Geophysics*, 72(1):S431–S48.

Stork, C. (1992). Reflection tomography in the postmigrated domain. *Geophysics*, 57(5):680–692.

Strikwerda, J. C. (1989). *Finite Difference Schemes and Partial Differential Equations*. Wadsworth & Brooks, California.

Tygel, M. and Hubral, P. (1989). Constant velocity migration in the various guises of plane-wave theory. *Surveys in Geophysics*, 10:331–348.

Tygel, M., Schleicher, J., and Hubral, P. (1996). A unified approach to 3-D seismic reflection imaging – Part II: Theory. *Geophysics*, 61(3):759–775.

Yan, L.-L. and Lines, L. (2001). Seismic imaging and velocity analysis for an Alberta Foothills seismic survey. *Geophysics*, 66(3):721–732.

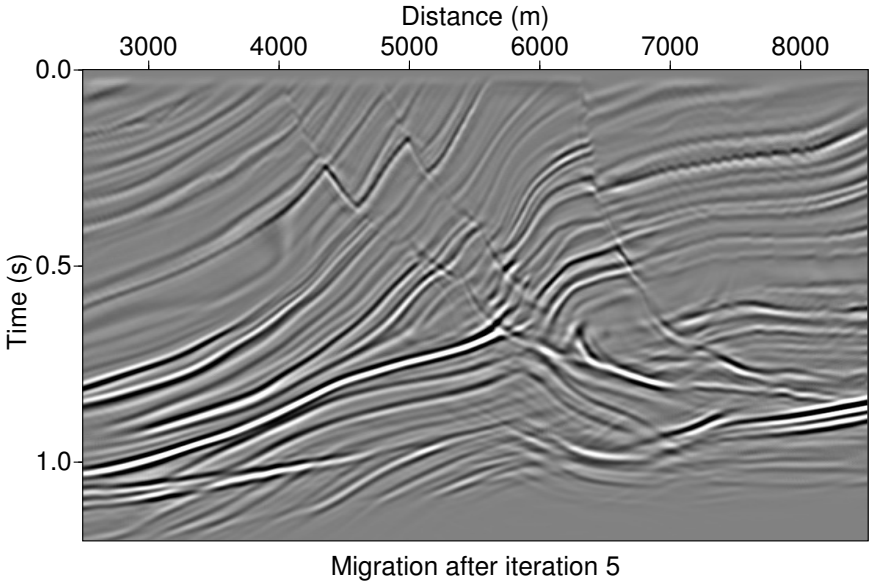

Figure 10: Final migrated image after velocity extraction using five iteration of image-wave RMO correction.

Yilmaz, Ö. (1987). *Seismic Data Processing*. Number 2 in Investigations in Geophysics. SEG, Tulsa, OK. (Doherty, S. M., Ed.).

Yilmaz, O. and Chambers, R. E. (1984). Migration velocity analysis by wave-field extrapolation. *Geophysics*, 49(10):1664–1674.

Zhu, J., Lines, L., and Gray, S. (1998). Smiles and frowns in migration/velocity analysis. *Geophysics*, 63(04):1200–1209.

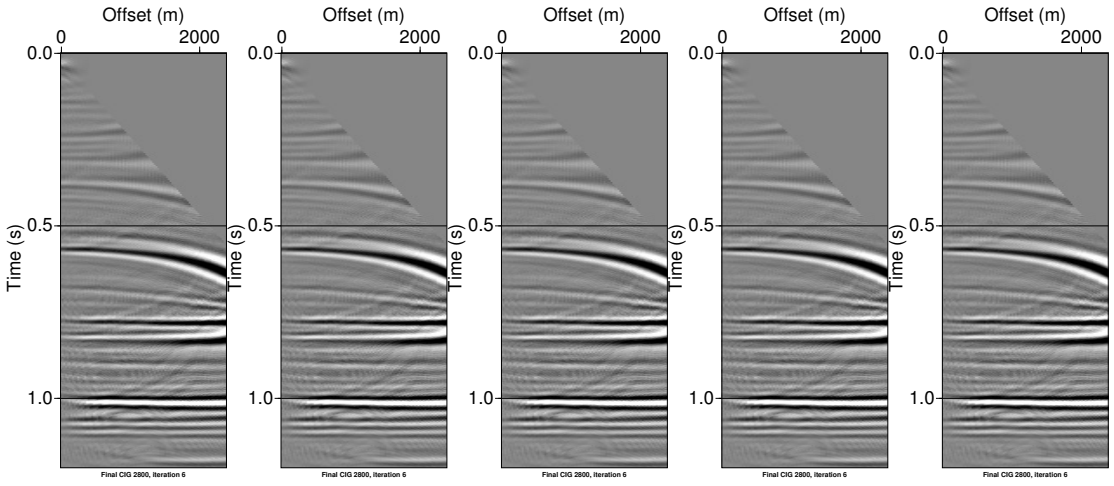

Figure 11: Common-image gathers correction at 2800 m, 4000 m, 5200 m, 6400 m, and 7600 m after final migration with the velocity model velocity extracted using five iterations of image-wave RMO correction.